Numerical Investigation of Extended Stern to Reduce Resistance of Planing Hull

Samuel Samuel[1], Parlindungan Manik[1], Rizal Kurnia Praja[1], Tuswan Tuswan[1], P. Paryanto[1], Mohamad Djaeni[1], Dian Purnama Sari[2]

The attributes of a high-speed vessel depend on various factors, such as trim angle, speed, center of gravity, and deadrise angle. The ship's trim angle will affect the ship's drag performance. Attempts to control trim have been made by adding stern appendages and modifying the hull. This study aims to analyze the performance of deep-V planing-hull ship drag by modifying the ship's stern. The stern modification investigation was carried out by adding length to the stern based on angles of 10^0, 20^0, and 30^0. This investigation evaluates resistance, trim, and heave while ignoring changes in ship displacement. The prediction of resistance and ship movements was simulated using the Reynold Averaged Navier-Stokes (RANS) equations to solve the problem. Numerical simulation applied the Computational Fluid Dynamics (CFD) based on finite volume method with an overset of techniques. Validation studies ensured numerical simulations have good accuracy based on comparisons with experimental model tests conducted by previous researchers. The pressure distribution caused by the extended stern affected the ship's drag, further demonstrating a better trim control. The results of the stern modification simulation revealed that the resistance was reduced at Fr 0.58–0.87. Extended sterns with an angle of 30° indicated the best results, with a resistance reduction percentage of 26% at Fr 0.58. However, drag increased at Fr speeds > 1.45 as the ship's speed increased.

KEY WORDS

~ Planing hull
~ Extended stern
~ Drag
~ CFD
~ Numerical simulation

[1] Diponegoro University, Faculty of Engineering, Semarang, Indonesia
[2] National Research and Innovation Agency, Surabaya, Indonesia
e-mail: samuel@ft.undip.ac.id
doi: 10.7225/toms.v13.n01.w03

Received: 12 Sep 2023 / Revised: 6 Nov 2023 / Accepted: 17 Nov 2023 / Published: 30 Nov 2023

1. INTRODUCTION

Trim in a planing hull is a critical factor that affects the performance, stability, and efficiency of a boat or high-speed vessel. Trim refers to the balance of the boat in the water, specifically the orientation of the boat's hull in relation to the waterline. Trim significantly affects the boat's speed and fuel efficiency. Achieving the correct trim allows the boat to ride on the water's surface more efficiently, reducing drag and enabling higher speeds with less power. Maintaining the correct trim reduces drag and resistance. When a boat is properly trimmed, the hull's shape is aligned optimally with the water's surface, reducing the resistance encountered as the boat moves through the water.

Planing Hulls are high-speed vessels with relatively complex hydrodynamic characteristics. Adding stern appendages such as interceptors, stern flaps or trim tabs, and hull vanes is an effort to improve fuel efficiency by reducing drag on the planing hull. Day and Cooper (2011) investigated how interceptors reduced drag on sailing yachts. The interceptor showed a 10–18% decrease in drag at 8–20 knots of speed. The evaluation of the interceptor is observed against the influential position to reduce the ship's drag. It is reported that the interceptor will reduce drag by controlling the moment caused by the interceptor (Samuel *et al.*, 2022). Yaakob *et al.*)2012) conducted tests on planing hull vessels using stern flaps, which reported an average drag reduction of 4.5%. Similar matters have been carried out to observe the performance of stern flaps or trim tabs (Budiarto *et al.*, 2022; Jadmiko *et al.*, 2018; Song *et al.*, 2018; Mansoori and Fernandes, 2017). Song *et al.* (2018) analyzed a combination of the interceptor and the stern flap that indicated a significant increase in resistance at Fr 0.334–0.058. Another study related to trim control is the hull vane, a transversely fixed foil at the transom bottom of a ship. Hull vane simulation aims to design energy-saving appendages to reduce ship drag with the help of Machine Learning and Artificial Neural Networks (Çelik *et al.*, 2021). The addition of stern appendages, such as interceptors, stern flaps or trim tabs, and hull vanes aims to control trim and reduce the ship’s drag.

Attempts to improve the resistance do not always employ the stern appendage but can also be made by modifying the hull shape. So far, various configurations such as chine (Hosseini *et al.*, 2021; Wheeler *et al.*, 2021; De Luca and Pensa, 2017), step hull (Najafi *et al.*, 2021; Najafi *et al.*, 2020; Park *et al.*, 2022; Vitiello *et al.*, 2022), spray rail (Olin *et al.*, 2017; Samuel *et al.*, 2021; Castaldi *et al.*, 2021), stern wedges (Ashkezari and Moradi, 2021), and tunnel (Atlar *et al.,* 2013; Yousefi *et al.,* 2014) have been researched to improve ship performance. Kim *et al.* (2013) developed three models of fast ship hulls using experimental methods. Deep-V Planing Straight (VPS), Deep-V Wave-Piercing Concave (VWC), and Deep-V Wave-Piercing Straight (VWS) were reported to have found out the effect of the ship's hull on the motion. Stern extending is carried out on each vessel but does not focus on hull modifications.

Yousefi *et al.* (2013) revealed the most popular CFD methods related to the planing hull, i.e. the Boundary Element Method (BEM), the Finite Element Method (FEM), and the Finite Volume Method (FVM). FVM is the most dominant method for predicting planing hull characteristics due to its better turbulence accuracy than other methods. Studies of the accuracy of turbulence models on ships have been conducted using k-epsilon and Detached Eddy Simulation (DES) approaches (Hosseini et al., 2021), while in the case of cylinders, it was carried out using k-epsilon approaches, i.e. the Reynolds Stress Model (RSM) and Large-Eddy Simulation (LES) (Kardan *et al.,* 2017). The research was done by Sukas *et al.* (2017) utilizing empirical, experimental, and CFD techniques. They report that ship motions may be predicted using the CFD approach and the overset mesh methodology.

Financial and environmental considerations to reduce fuel consumption are becoming a necessity. Based on previous research, efforts to improve the ship’s drag were carried out by adding a stern appendage and modifying the hull form. The addition of a stern appendage aims to provide a lift on the stern at a certain speed. The speed has a strong influence on the pressure in the extended stern of the ship, so designers can use this knowledge to make a compensation between the drag and the hull shape. This study aimed to modify

the ship's stern by adding an extended stern. The increase in the length of the vessel at the stern affects the angle of the trim; thus, it improves the drag at a certain speed. This study examined the effect of an extended stern on planing-hull ships. This research verified the results of the CFD simulation using Park *et al.* (2019) experiment in calm water conditions. Numerical simulations were performed using the Reynold Averaged Navier-Stokes (RANS) equation to solve fluid dynamics. The air-water flow around the hull acts on calm water and is assumed to be fixed in roll and free in heave and pitch directions.

2. MATERIAL AND METHOD

2.1. Research Object

Aragon 2 is a 6th generation hull development from (Kim and Kim, 2017a). The Korea Research Institute of Ships and Ocean Engineering (KRISO) designed the ship full-scale without passengers for military purposes. Turning characteristic testing has been attempted by (Kim and Kim, 2017b). The object used in this research is Aragon 2 hull form which is simulated in calm water conditions. The ship data is a scale model that has been tested experimentally by Park *et al.* (2019). The CFD model uses a 1/5.33 scale with details of the main sizes in Table 1. 3D modeling, experimental, and full-scale Aragon 2 are shown in Figure 1.

Dimension	Full Scale	Model Scale 1/5.33	Unit
Length Overall (LOA)	8.00	1.50	meter
Length at Waterline (LWL)	7.53	1.41	meter
Breadth (B)	2.20	0.41	meter
Draft (T)	0.41	0.07	meter
Displacement (Δ)	3000	19.78	kg
LCG	2.64	0.49	meter
C. G from baseline	0.80	0.15	meter
Deadrise angle		16 at transom, 24 at midship	degree

Table 1. Principal dimensions of the ship.

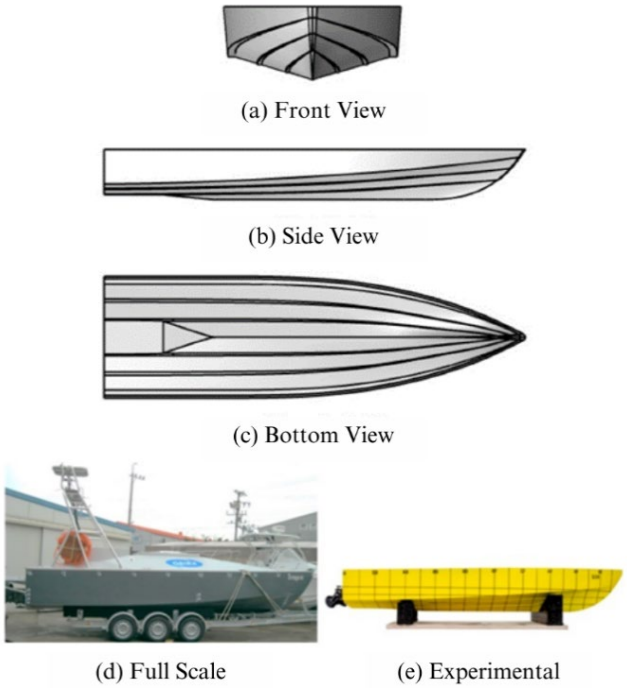

Figure 1. (a) Front view, (b) Side view, (c) Bottom view, (d) Full scale, and (e) Experimental of Aragon 2 hull form.

2.2. Research Method

This study aimed to analyze ship's drag, trim, and heave due to different forms of the extended stern. The extended stern variation using different angles is visualized in Figure 2. The extended stern underside was a modification to the stern of the ship to reduce the total drag and the required trim angle at high speeds to improve the ship's performance. CFD simulation will be carried out based on Table 2.

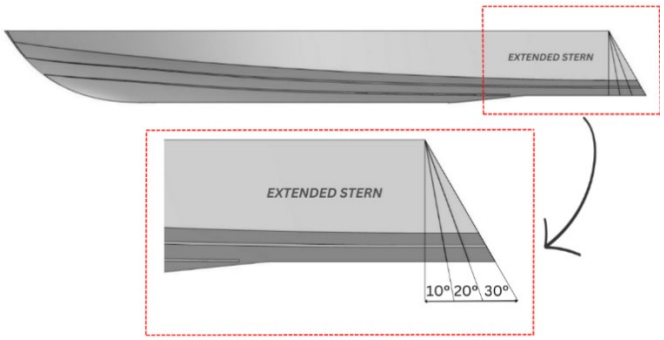

Figure 2. Extended stern variations.

Parameter	Variable
Extended Stern angle	10° 20° 30°
Froude Number	0.29; 0.58; 0.87; 1.16; 1.45

Table 2. Model Variations

The domain size and boundary conditions refer to the ITTC recommendation (ITTC, 2014). Figure 3 illustrates the size of the computational domain and boundary conditions. Based on the length between perpendiculars (L), the domain length was measured from −2.5 L to 1 L with the coordinates of the zero point at the stern and the vessel's draft. The width was set to 1.5 L and the water depth was 2 L. The inflow, bottom, side, and top flow limits were described with inlet velocity; the outlet limits were pressure outlets placed far enough away to ensure that no flow reflection occurred, and the fluid could fully expand. The body surface employed a no-slip limit condition. The simulation was carried out on half the hull, it was modeled to save computational time. Normal velocity and gradient variables were zero in the symmetry plane condition.

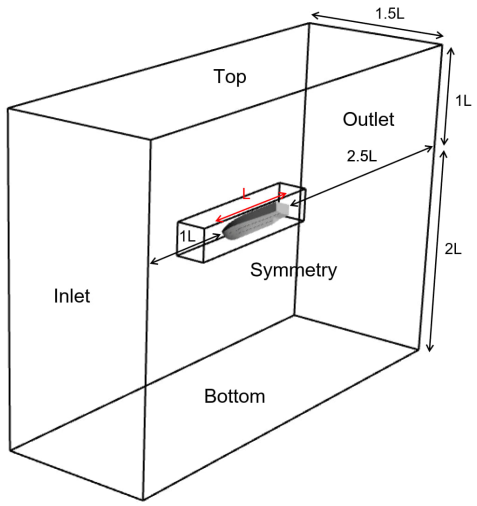

Figure 3. Computational domain and boundary condition.

Prism layers were made adjacent to the hull to catch the flow of boundary layers accurately, and six prism layers were used in this study. The wall function (y+) was used to reduce inaccuracies in calculations, y+ value between 30-130 to get accurate results (Suneela *et al.*, 2021). Meanwhile, according to ITTC recommendations, the value of y+ can be calculated using Eq. (1).

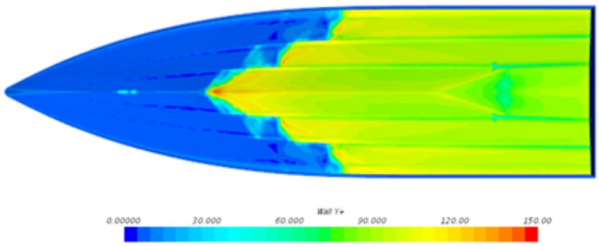

Figure 4. Wall y+.

$$Y^{+} = \frac{(\rho \,.\, U \,.\, y)}{\mu} \tag{1}$$

Where U is the friction velocity at the wall, y is the distance from the wall to the first grid node, and μ is the dynamic viscosity of the fluid. Figure 4 shows y+ values on ships, where the average y+ values were 50–100. The time step was the space between each computation iteration. The time step employed for this simulation was a function of the ship's speed (V) and waterline length (L) according to Eq. (2), as recommended by ITTC. The Courant-Friedrichs-Lewy (CFL) number was used to determine the time step in this investigation. The CFL

value represented the total distance that the fluid particles had covered in a given period. A smaller time step is employed when the ship is moving more quickly. This study took the average time step value of 0.008, as shown in Figure 5.

$$\Delta t \, \mathrm{ITTC} = 0.005 \sim 0.01 \, \frac{\mathrm{L}}{\mathrm{V}} \tag{2}$$

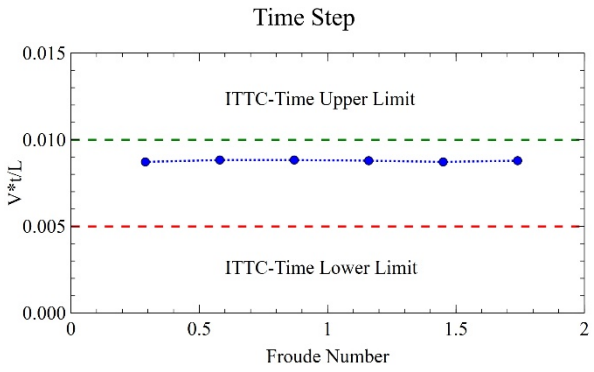

Figure 5. Time-Step.

2.3. Numerical Approach

In this study, a method called computational fluid dynamics (CFD) is used to simulate a ship model. The simulation relies on the unsteady Reynolds-Averaged Navier-Stokes equations, a problem-solving approach based on the conservation of mass and momentum principles, to conduct the hydrodynamic simulation (Kinaci *et al.*, 2016). Here is the URANS equation.

$$\frac{\partial U_i}{\partial x_i} = 0 \tag{3}$$

$$\frac{\partial U_i}{\partial t} + \frac{\partial (U_i U_j)}{\partial x_j} = -\frac{1}{\rho}\frac{\partial P}{\partial x_i} + \frac{\partial}{\partial x_i}\left(2\nu S_{ij} - \overline{u_i' u_j'}\right) \tag{4}$$

Where U_i and u_i' express the mean and fluctuation velocity component in the direction of the Cartesian coordinate x_i, P is the mean pressure, ρ is the density, ν is the molecular kinematic viscosity and S_{ij} is the mean strain-rate tensor. The strain-rate tensor is defined as

$$S_{ij} = \frac{1}{2}\left(\frac{\partial U_i}{\partial x_j} + \frac{\partial U_j}{\partial x_i}\right) \tag{5}$$

The last term on the right-hand side of Eq. (4) is denoted as the Reynolds stress tensor, which is given by

$$\tau_{ij} = \overline{u_i' u_j'} = \mu_t \left(\frac{\partial U_i}{\partial x_j} + \frac{\partial U_j}{\partial x_i} - \frac{1}{3}\frac{\partial U_k}{\partial x_k}\partial_{ij}\right) - \frac{2}{3}\rho k \partial_{ij} \tag{6}$$

The Boussinesq (eddy-viscosity) hypothesis obtained with the $k-\varepsilon$ turbulence model is expressed by

$$\mu_t = \frac{1}{2}\frac{\rho \tau_{ij}}{S_{ij}} \tag{7}$$

The k-ε turbulence model specifies that the turbulent eddy viscosity is calculated by

$$\mu_t = c_\mu \rho \frac{k^2}{\varepsilon} \tag{8}$$

The turbulent kinetic energy k and the rate of dissipation of the turbulent energy ε are calculated below

$$\frac{\partial \rho k}{\partial t} + \frac{\partial \rho U_j k}{\partial x_j} = \frac{\partial}{\partial x_j} + \left[\left(\mu + \frac{\mu_t}{\sigma_t}\right)\frac{\partial k}{\partial x_j}\right] + P_k - \rho\varepsilon \tag{9}$$

$$\frac{\partial \rho \varepsilon}{\partial t} + \frac{\partial \rho U_j \varepsilon}{\partial x_j} = \frac{\partial}{\partial x_j} + \left[\left(\mu + \frac{\mu_t}{\sigma_\varepsilon}\right)\frac{\partial \varepsilon}{\partial x_j}\right] + \frac{\varepsilon}{k}(c_{\varepsilon 1} P_k - c_{\varepsilon 2}\rho\varepsilon) \tag{10}$$

2.4. Overset Mesh Technique

The overset mesh technique was employed for meshing in this investigation. A mesh technique called overset mesh or overlapping grids uses the donor-acceptor cells technique. There are two geometries: overset as a donor receiver and background as a donor. The primary emphasis has been placed on solving the governing equations using overlapping grids. Special aspects related to integrating inter-grid coupling into the global solution procedure and ensuring mass conservation at overlapping interfaces were developed. This approach offers numerous advantages in the computation of problems involving multiple bodies, moving bodies, and optimization studies.

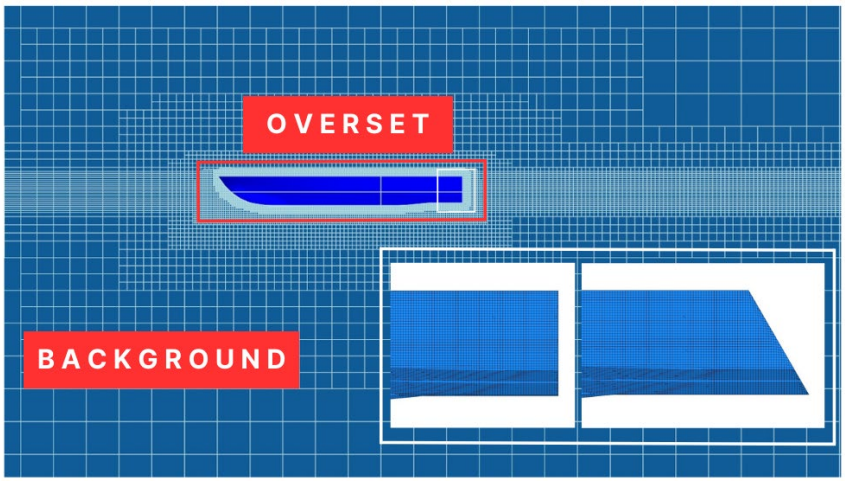

Figure 6. Mesh Density.

De Luca *et al.* (2016) research compared the overset grid and moving grid methods. As a result, an overset grid displayed better results than a moving grid. De Marco *et al.* (2017) compared the overset grid method with morphing grid, both showed promising results, but the overset grid was slightly better at accurately predicting outcomes. However, overset grid took a long time because of the two interconnected boundaries. The concentration of the mesh was carried out based on x, y, and z coordinates using isotropic or anisotropic methods. The denser the mesh concentration, the more computational time it takes; hence, the mesh density is only done in certain parts. The visualization of mesh density in this study is shown in Figure 6.

3. RESULT AND DISCUSSION

3.1. Verification of Experiments and CFD

In essence, a model is converted into computer code, allowing the CFD simulation to be executed and producing data for engineering study. The process of verification and validation involves scrutinizing both the code and simulation results to identify any errors. Table 3 shows studies of grid independence aimed at selecting grid quality. These grid mesh materials are manufactured in five different mesh, i.e. 0.40; 0.69; 1.02; 1.55, and 2.01 million cells, with a Froude number of 1.45. Resistance was visualized with non-dimensional units R/Δ, trim with degrees, and heave with non-dimensional units rise of cg/draft. Ahmed and El-Ela (2023) compare experimental and computational results. The results show that the resistance values at various speeds for the fine mesh show a very good and improved agreement with the experimental data, with an error of less than 6%. This indicates that CFD model is capable of simulating the steady flow around the ship's hull with an acceptable accuracy and thus can be used as a complementary tool to laboratory model tests for ship design and ship hydrodynamic research (Ahmed, 2023). It was carried out to ensure that the data obtained has converged; thus, this research can be declared valid.

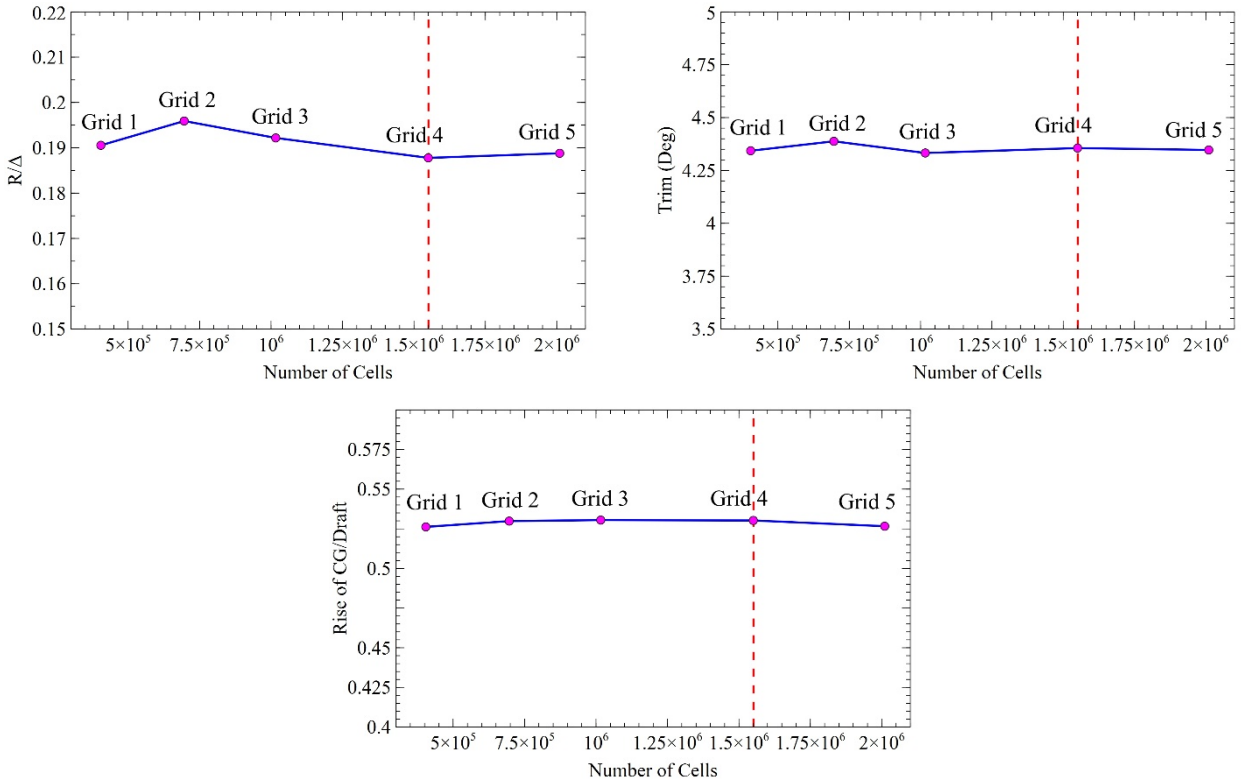

Figure 7. Grid independence of drag, trim, and heave.

The graph indicates that the data converge as the number of meshes increases, as shown in Figure 7. The results of grids 4 and 5 reveal good value stability. However, grid 5 requires longer computing time. Hence, the simulation in this study used grid 4 with a total mesh of 1.55M and a large percentage of error for resistance of 8.89%, trim of 5.97%, and heave of 12.97% in comparison, considering computational cost with convergence results.

No	Mesh Quality	Number of Cells
1	Very Coarse	404,474
2	Coarse	696,084
3	Medium	1,016,192
4	Fine	1,550,408
5	Very Fine	2,010,230

Table 3. Mesh Number of Cells.

The convergence of model data for resistance, trim, and heave values was evaluated with physical time, indicating the data converged after 4 seconds. The convergence of data over time is shown in Figure 8.

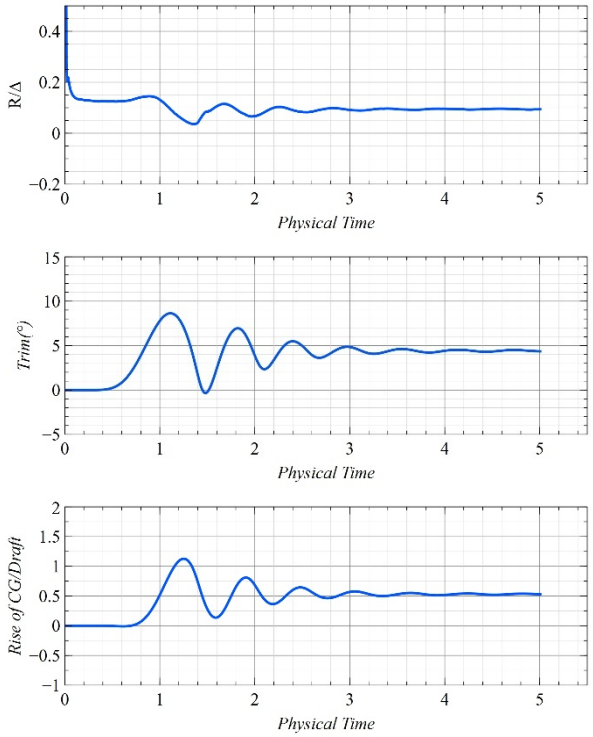

Figure 8. The convergence of hydrodynamic characteristics in time.

3.2. Validation Benchmark

The validation of this study used the results of Park *et al.* (2019) experiment in calm water conditions. The pattern formed between the results of CFD, and the experiment indicates that the results are as presented in Figure 9. However, there was still a difference in the calculation with the experiment results; this happened because of the limitations of modeling an object in numerical computing and the conditions during the experiment in the towing tank. Similar cases also occurred in Song *et al.* (2018) study, with an average error for resistance of 2.65% and trim and sinkage of 9.45% and 7.96% respectively. This study had an average error for resistance of 8.92%, trim and heave of 3.80% and 12.3%, respectively, at all speed variations.

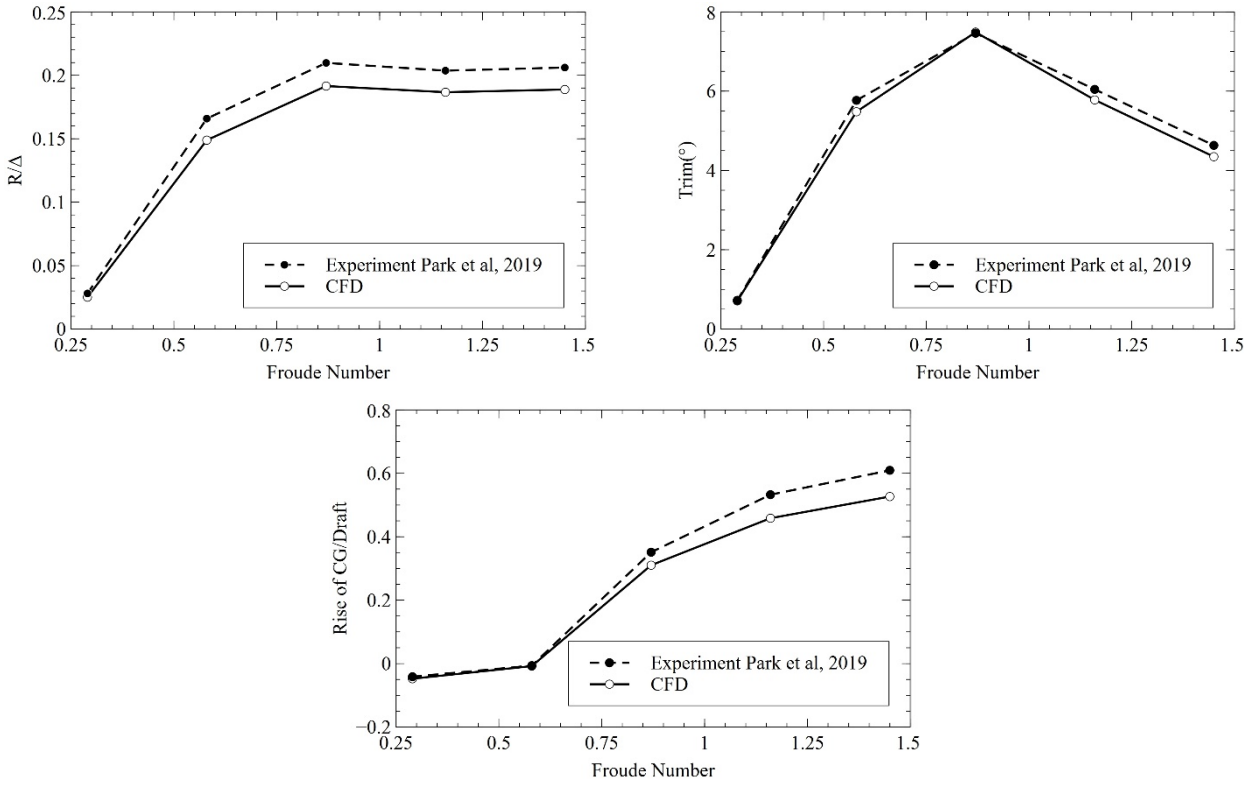

Figure 9. Graph validation of drag, trim, and heave between CFD and experiment.

3.3. Simulation Result

Ships moving on the water created water flow from the front to the stern hull. The waves generated due to the flow of water that hit the front of the ship passed through the middle of the ship. Then, it led to the back of the ship, which made the phenomenon of water flow at the back of the ship due to the change in the flow speed generated from the front. Therefore, the choice of the shape of the stern hull also greatly affects the flow of water behind the ship. In addition, the determination of the shape of the stern hull significantly influences the magnitude of the ship's resistance value. Figure 10 illustrates the reduced drag, trim, and heave values associated with various extended stern shapes at angles of 10°, 20°, and 30°. By increasing speed, resistance will increase followed by trim, but at Fr 0.8 there is a "hump" region phenomenon so that trim increases significantly, which causes resistance to increase, too. These findings also show that on a planing ship there are three regions, namely displacement mode, transition mode and planing mode.

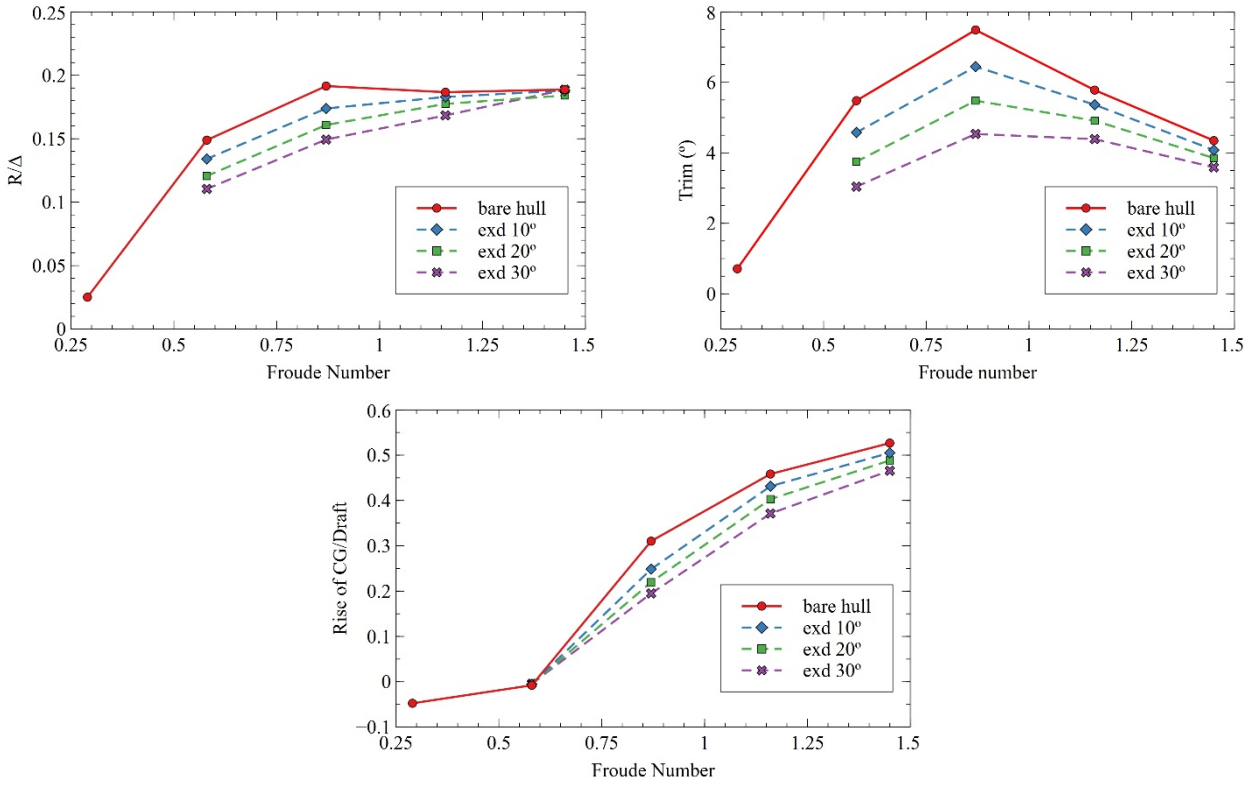

Figure 10. The effect of the extended stern on total resistance, trim, and heave.

A vessel frictional resistance (R_F) and pressure resistance (R_P) are computed using a RANS solver to create tangential and normal forces. R_P is a normal force operating on the surface of the ship, while (R_F) is a force that acts tangentially. R_P can be further divided into viscous resistance (R_{VP}) and wave-making resistance (R_W). The following equation defines total resistance:

$$R_T = R_F + R_P \tag{11}$$

$$R_T = R_F + (R_W + R_{VP}) \tag{12}$$

$$C_T = R_T / 0.5 \, x \, \rho \, x \, WSA \, x \, Vs^2 \tag{13}$$

Meanwhile, the resistance coefficient based on ITTC is shown in Eq. 13. Where R_T is the dimensional resistance for the total resistance component, ρ is the density of the fluid, WSA is the wetted surface area, and Vs is the vessel's velocity. Table 4 shows drag components at Fr 0.58.

	Bare Hull	Exd 10°	Diff (%)	Exd 20°	Diff (%)	Exd 30°	Diff (%)
R_F[N]	4.07	4.27	5%	4.31	6%	4.51	11%
R_{VP}[N]	11.08	10.87	-2%	6.86	-38%	6.71	-39%
R_W[N]	14.18	11.36	-20%	12.68	-11%	10.55	-26%
R_T[N]	29.33	26.51	-10%	23.85	-19%	21.77	-26%

Table 4. Drag components.

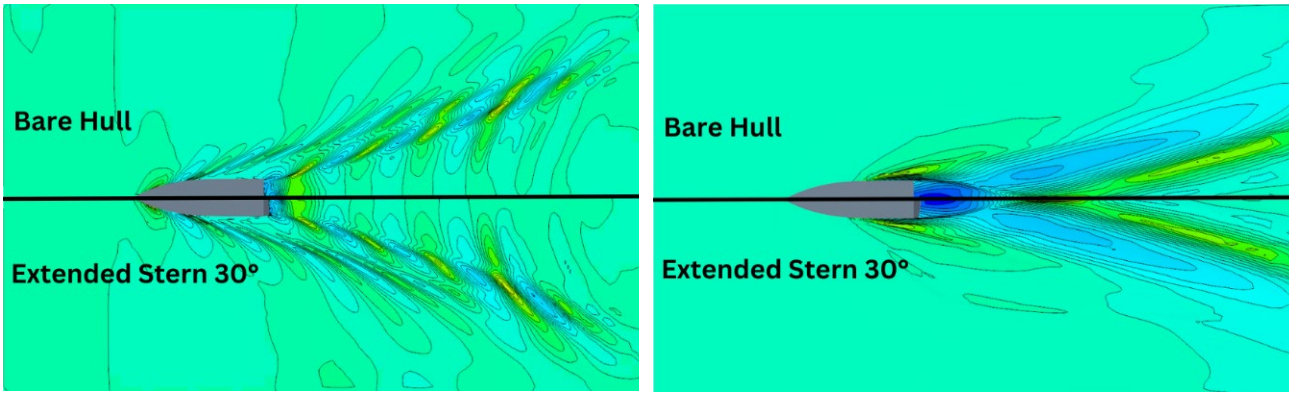

a. b.

Figure 11. Wave pattern (a) Fr 0.29 and (b) Fr 1.16.

Table 4 compares the vessel's total drag and components on a bare hull and extended stern 30° at Fr 0.58. Frictional Resistance (R_F) increased by 11% due to the addition of the wetted surface area (WSA) with extended stern on planing-hull vessels. On the other hand, it is observed that wave-making resistance (R_W) and viscous resistance (R_{VP}) decreased due to extended stern. The extensive pressure distribution towards the stern reduced the waves at the ship's stern. The change in wave at the stern due to the influence of the extended stern is depicted in Figure 11 at Fr 0.29 and 1.16. As a result, wave-making resistance (R_W) and total resistance (R_T) were reduced by 26%.

The graph shows that the effective reduction occurs in the transition mode/semi-planing phase of the planing-hull ship, which was between Fr 0.58 – 0.87. At a 10° extended stern angle, the best resistance and trim reduction percentages were 10% and 16% at Fr 0.58 respectively; the heave was 20% at Fr 0.87. The 20° extended stern angle indicates a more significant percentage reduction at Fr 0.58 of 19% and 32% for resistance and trim respectively; the heave was 29% at Fr 0.87. The extended stern with an angle of 30° showed the best results of the previous two variations with resistance and trim reduction percentages of 26% and 45% respectively at Fr 0.58, as well as heave, the percentage reduction of 37% at Fr 0.87.

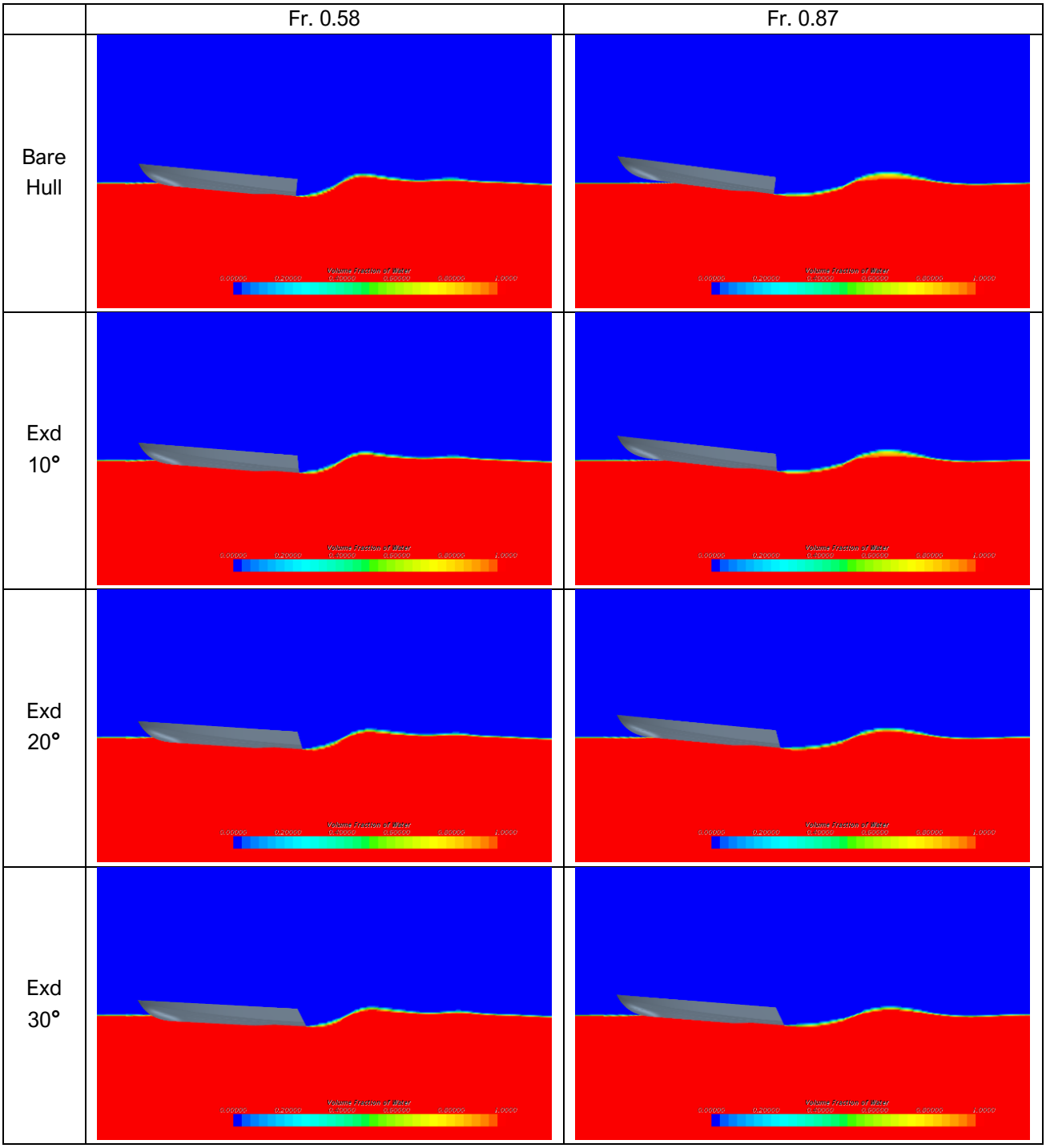

Figure 12. Visualization of trim on Froude number 0.58 and 0.87.

The shape of the water surface stern of the ship at Fr 0.58 and 0.87 is shown in Figure 12. The figure illustrates a significant improvement in trim angle as the speed and angle of the extended stern increase. The larger the angle, the greater the effectiveness for reducing drag, trim, and heave. However, it caused problems at high speeds or Fr more than 1.45. The graph at high speeds will only increase the ship's drag, thus losing its effectiveness.

Pressure distribution on bare-hull ships and ships with extended sterns is shown in Figure 13. It was observed that the pressure on ships with extended sterns was lower compared to bare hulls. The pressure

distribution decreased from the high-pressure area in the bow to the stern affecting the trim. Pressure on the stern creates lift and reduces the trim of the ship.

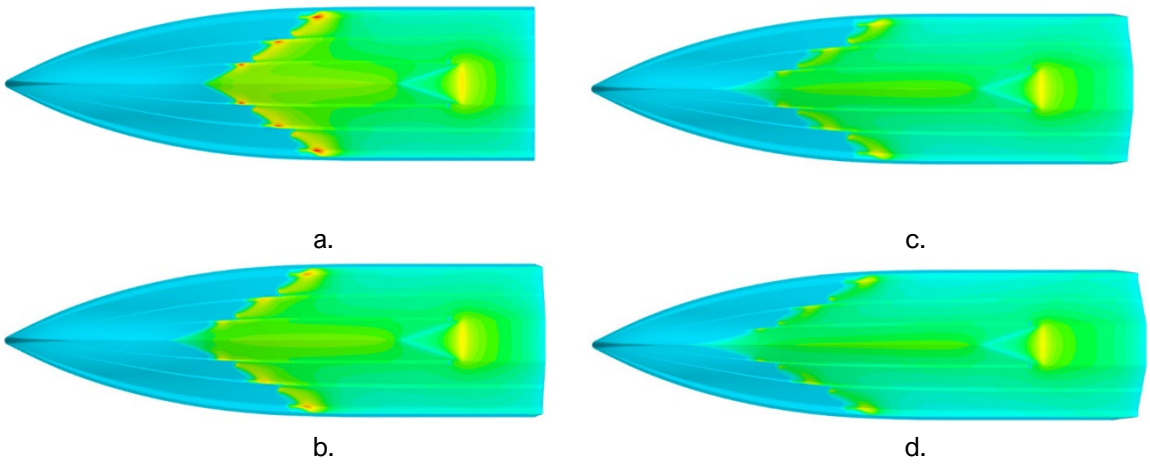

Figure 13. Pressure distribution (a) bare hull and extended stern (b) 10°, (c) 20°, and (d) 30° at Fn 0.87.

4. CONCLUSION AND FUTURE WORK

This study aims to determine how various extended stern shapes with angles of 10°, 20°, and 30° affect the hydrodynamic performance of ships. According to the research findings, the orientation of the extended stern exerts a noteworthy influence on the vessel's resistance, trim, and vertical movements. The best performance improvement is in the semi-planing / transition mode phase at Fr 0.58 – 0.87. The results showed that ships with an extended stern angle of 30° indicated a percentage of drag reduction of up to 26%, trim 45% at Fr 0.58, and heave 37% at Fr 0.87. This research was limited to Aragon 2 ships and at certain speeds; for use at high speeds (> Fr 1.45), the effect of extending the stern needs further study.

Using an extended stern can provide a fuel reduction solution related to the EEDI coefficient considered at the ship design stage, at least consistently good for reducing exposure to carbon dioxide. This study is the initial study to predict the drag of ships that will use interceptors on different stern shapes. This will demonstrate the relationship between the interceptor and the hull to be discussed in future research. When modifying a planing hull by adding a stern extension, the shift in the Longitudinal Center of Gravity (LCG) due to the change in the hull's length is indeed an important consideration. Observations about LCG points need to be considered to obtain good results.

ACKNOWLEDGMENTS

The authors gratefully acknowledge financial support from Universitas Diponegoro for this work under the project scheme of *Development and Application Research* (RPP) 225-08/UN7.D2/PP/IV/2023.

CONFLICT OF INTEREST: The authors declared no potential conflicts of interest with respect to the research, authorship and publication of this article.

REFERENCES

Ahmed, A.M.E., 2023. Comparative Investigation of Resistance Prediction for Surface Combatant Ship Model using CFD Modeling. Journal of Advanced Research in Fluid Mechanics and Thermal Sciences, 107(2), pp. 225–235.

Ahmed, A.M.E. and El-Ela, A.M.A., 2023. Experimental and CFD Resistance Validation of Naval Combatant DTMB 5415-51 Model. Journal of Advanced Research in Fluid Mechanics and Thermal Sciences, 107(2), pp .84–102.

Ashkezari, A.Z. and Moradi, M., 2021. Three-dimensional simulation and evaluation of the hydrodynamic effects of stern wedges on the performance and stability of high-speed planing monohull craft. Applied Ocean Research, 110, p.102585. Available at: https://doi.org/10.1016/j.apor.2021.102585.

Atlar, M. et al., 2013. Anti-slamming bulbous bow and tunnel stern applications on a novel Deep-V catamaran for improved performance. International Journal of Naval Architecture and Ocean Engineering, 5(2), pp. 302–312. Available at: https://doi.org/10.3744/JNAOE.2013.5.2.302.

Budiarto, U. et al., 2022. Stern Flap Application on Planing Hulls to Improve Resistance. International Journal of Engineering, 35(12), pp. 2313–2320. Available at: https://doi.org/10.5829/IJE.2022.35.12C.06.

Castaldi, L. et al., 2021. The effect of spray deflection on the performance of high speed craft in calm water. Ocean Engineering, 229, 108892.

Çelik, C. et al., 2021. A reduced order data-driven method for resistance prediction and shape optimization of hull vane. Ocean Engineering, 235, 109406. Available at: https://doi.org/10.1016/j.oceaneng.2021.109406.

Day, A.H. and Cooper, C., 2011. An experimental study of interceptors for drag reduction on high-performance sailing yachts. Ocean Engineering, 38, pp. 983–994. Available at: https://doi.org/10.1016/j.oceaneng.2011.03.006.

Hosseini, A. et al., 2021. Performance Prediction of a Hard-Chine Planing Hull by Employing Different CFD Models. Journal of Marine Science and Engineering, 9(5), 481. Available at: https://doi.org/10.3390/jmse9050481.

Jadmiko, E., Arief, I.S. and Arif, L., 2018. Comparison of Stern Wedge and Stern Flap on Fast Monohull Vessel Resistance. International Journal of Marine Engineering Innovation and Research, 3(2), pp. 41–49. Available at: https://doi.org/10.12962/j25481479.v3i2.4601.

Kardan, N., Hakimzadeh, H. and Hassanzadeh, Y., 2017. Investigation of the Dynamics Bed Shear Stress Distribution around a Circular Cylinder Using Various Turbulences Models. Engineering Journal, 21(7), pp.75–86. Available at: https://doi.org/10.4186/ej.2017.21.7.75.

Kim, D.J. et al., 2013. Design of high-speed planing hulls for the improvement of resistance and seakeeping performance. International Journal of Naval Architecture and Ocean Engineering, 5(1), pp.161–177. Available at: https://doi.org/10.2478/ijnaoe-2013-0124.

Kim, D.J. and Kim, S.Y., 2017a. Comparative Study on Manoeuvring Performance of Model and Full-scale Waterjet Propelled Planing Boats. *FAST*. 2017 Nates-France, pp. 126–135.

Kim, D.J. and Kim, S.Y., 2017b. Turning characteristics of waterjet propelled planing boat at semi-planing speeds. Ocean Engineering, 143, pp. 24–33. Available at: https://doi.org/10.1016/j.oceaneng.2017.07.034.

Kinaci, O.K., Sukas, O.F. and Bal, S., 2016. Prediction of wave resistance by a Reynolds-averaged Navier-Stokes equation-based computational fluid dynamics approach. Proceedings of the Institution of Mechanical Engineers Part M: Journal of Engineering for the Maritime Environment, 230(3), pp. 531–548.

De Luca, F. et al., 2016. An Extended Verification and Validation Study of CFD Simulations for Planing Hulls. Journal of Ship Research, 60(2), pp. 101–118. Available at: https://doi.org/10.5957/JOSR.60.2.160010.

De Luca, F. and Pensa, C., 2017. The Naples warped hard chine hulls systematic series. Ocean Engineering, 139, pp. 205–236. Available at: https://doi.org/10.1016/j.oceaneng.2017.04.038.

Mansoori, M. and Fernandes, A.C., 2017. Interceptor and trim tab combination to prevent interceptor's unfit effects. Ocean Engineering, 134, pp. 140–156.

De Marco, A. et al., 2017. Experimental and numerical hydrodynamic analysis of a stepped planing hull. Applied Ocean Research, 64, pp. 135–154. Available at: https://doi.org/10.1016/j.apor.2017.02.004.

Najafi, A., Nowruzi, H. and Ameri, M.J., 2020. Hydrodynamic assessment of stepped planing hulls using experiments. Ocean Engineering, 217(424), pp. 107939. Available at: https://doi.org/10.1016/j.oceaneng.2020.107939.

Najafi, A. et al., 2021. An experimental study of the wetted surfaces of two- stepped planing hulls. Ocean Engineering, 222(424), pp. 108589. Available at: https://doi.org/10.1016/j.oceaneng.2021.108589.

Olin, L. et al., 2017. Numerical modelling of spray sheet deflection on planing hulls. Proceedings of the Institution of Mechanical Engineers Part M: Journal of Engineering for the Maritime Environment, 231(4), pp. 811–817.

Park, J.Y. et al., 2019. An experimental study on vertical motion control of a high-speed planing vessel using a controllable interceptor in waves. Ocean Engineering, 173, pp. 841–850. Available at: https://doi.org/10.1016/j.oceaneng.2019.01.019.

Park, S. et al., 2022. Single- and two-phase CFD V&V for high-speed stepped planing hulls. Ocean Engineering, 261, 112047. Available at: https://doi.org/10.1016/j.oceaneng.2022.112047.

Samuel, S. et al., 2022. Evaluation of Interceptor Design To Reduce Drag On Planing Hull. Brodogradnja, 73(3), pp. 93–110. Available at: https://doi.org/10.21278/brod73306.

Samuel, S. et al., 2021. A Numerical Study of Spray Strips Analysis on Fridsma Hull Form. Fluids, 6(11), 420. Available at: https://doi.org/10.3390/fluids6110420.

Song, K. et al., 2018. Influence of interceptors, stern flaps, and their combinations on the hydrodynamic performance of a deep-vee ship. Ocean Engineering, 170, pp.306–320. Available at: https://doi.org/10.1016/j.oceaneng.2018.10.048.

Sukas, O.F., Kinaci, O.K., Cakici, F. and Gokce, M.K., 2017. Hydrodynamic assessment of planing hulls using overset grids. Applied Ocean Research, 65, pp. 35–46. Available at: https://doi.org/10.1016/j.apor.2017.03.015.

Suneela, J., Krishnankutty, P. and Subramanian, V.A., 2021. Hydrodynamic performance of planing craft with interceptor-flap hybrid combination. Journal of Ocean Engineering and Marine Energy, 7(4), pp. 421–438. Available at: https://doi.org/10.1007/s40722-021-00211-0.

Vitiello, L. et al., 2022. A comprehensive stepped planing hull systematic series: Part 1 - Resistance test. Ocean Engineering, 266, 112242. Available at: https://doi.org/10.1016/j.oceaneng.2022.112242.

Wheeler, M.P., Matveev, K.I. and Xing, T., 2021. Numerical Study of Hydrodynamics of Heavily Loaded Hard-Chine Hulls in Calm Water. Journal of Marine Science and Engineering, 9(2), 184. Available at: https://doi.org/10.3390/jmse9020184.

Yaakob, O., Shamsuddin, S. and Koh, K.K., 2012. Stern Flap for Resistance Reduction of Planing Hull Craft: A Case Study with a Fast Crew Boat Model. Jurnal Teknologi, 41, pp. 43–52. Available at: https://doi.org/10.11113/jt.v41.689.

Yousefi, R., Shafaghat, R. and Shakeri, M., 2014. High-speed planing hull drag reduction using tunnels. Ocean Engineering, 84, pp. 54–60. Available at: https://doi.org/10.1016/j.oceaneng.2014.03.033.

Yousefi, R., Shafaghat, R. and Shakeri, M., 2013. Hydrodynamic analysis techniques for high-speed planing

hulls. Applied Ocean Research, 42, pp. 105–113. Available at: https://doi.org/10.1016/j.apor.2013.05.004.